Article

Not peer-reviewed version

Carbonized Melamine Cyanurate as a Palladium Catalyst Support for the Dehydrogenation of N-heterocyclic Compounds in LOHC Technology

Anton P. Koskin *, Yurii V. Larichev, Sergey A. Stepanenko, Yury V. Dubinin, Artem B. Ayupov, Evgeny A. Suprun, Petr M. Yeletsky *

Posted Date: 6 July 2023

doi: 10.20944/preprints202307.0410.v1

Keywords: g-C3N4; melamine cyanurate; Pd catalysts; single atom catalysts; hydrogen storage; LOHC; dehydrogenation

Article

Carbonized Melamine Cyanurate as a Palladium Catalyst Support for the Dehydrogenation of N-Heterocyclic Compounds in LOHC Technology

Anton P. Koskin, Yurii V. Larichev, Sergey A. Stepanenko, Yury V. Dubinin, Artem B. Ayupov, Evgenii A. Suprun and Petr M. Yeletsky *

Federal Research Center Boreskov Institute of Catalysis, Siberian Branch of the Russian Academy of Sciences, Prospekt Akademika Lavrentieva 5, Novosibirsk, 630090, Russia

* Correspondence: yeletsky@catalysis.ru

Abstract: In this work, the use of graphite-like carbon nitride (g-C_3N_4) with improved texture characteristics for the synthesis of supported palladium catalysts of dehydrogenation of nitrogen-containing heterocycles was studied. This process is key to the creation of liquid organic carrier technology (LOHC) using N-heterocycles as reversibly hydrogenated/dehydrogenated substrates. For the preparation of g-C_3N_4-mca supports with advanced textural characteristics, well-established technology of the melamine cyanurate complex carbonization and standard techniques of adsorption precipitation together with wet impregnation were used for the synthesis of Pd-containing systems. The activity of the synthesized catalysts was studied in decahydroquinoline dehydrogenation. The high weight content of extractable hydrogen (7.2 wt %) and the high extraction rate, respectively, make it possible to consider these substances as the most promising N-heterocyclic compounds for this technology. It was shown that an increase in the specific surface area of g-C_3N_4 allows for achieving a slightly lower, but comparable fineness of palladium particles for the 1 wt% Pd/MCA-500 sample, compared to the standard 1 wt% Pd/C. In this case, the catalytic activity of 1 wt% Pd/MCA-500 in dehydrogenation of both substrates exceeded the analogous parameter for catalysts supported by nitrogen free supports. This regularity is presumably associated with the electron-donor effect of surface nitrogen, which favorably affects the dehydrogenation rate as well as the stability of catalytic systems.

Keywords: g-C_3N_4; melamine cyanurate; Pd catalysts; single atom catalysts; hydrogen storage; LOHC; dehydrogenation

1. Introduction

The development of hydrogen energy, as an alternative to the use of hydrocarbon fuels, implies the development of environmentally friendly methods for the synthesis of H_2 and the creation of technologies for its storage and transportation. One of the most promising hydrogen storage/transport technologies, at this moment, is the technology of liquid organic hydrogen carriers (LOHC) [1,2]. Herewith, among LOHC substrates, N-containing heterocycles, such as indole [3,4] and quinoline [5,6] derivatives, attract increasing attention due to their lower hydrogenation/dehydrogenation enthalpy compared to cyclic hydrocarbons.

In recent years, an environmentally friendly method of hydrogen production via photocatalytic water splitting has been actively studied [7,8] when considerable attention is paid to the use of graphite-like carbon nitride (g-C_3N_4) as a photocatalyst for this process [9]. Carbon nitride is a rare example of a non-metallic semiconductor material that has such important advantages as the relative ease of synthesis, as well as good biocompatibility and inexpensiveness [10]. Along with the photocatalytic applications of g-C_3N_4, other ones using carbon nitride as a support for metal-supported catalysts are also being actively developed. In this case, g-C_3N_4 has all the advantages of N-doped mesoporous carbonaceous materials [11]. In particular, stabilization of the deposited metal

 doi:10.20944/preprints202307.0410.v1

component in a highly dispersed state and the resistance of metals to the leaching during the catalytic transformation are achieved due to the interaction of the metal with surface nitrogen. Supported catalysts containing palladium are currently being actively investigated in dehydrogenation of H_2-saturated N-heterocycles [12]. This process is a key one in a promising hydrogen storage technology using N-heterocycles as LOHC substrates. When implementing this technology, hydrogen is being accumulated through the catalytic hydrogenation of a N-heterocycle (H_2-lean form of the LOHC substrate) and, subsequently, is being extracted as a result of the dehydrogenation of the nH-N-heterocycle (H_2-rich form). It has been repeatedly shown that the use of carbonaceous supports, compared to oxidic ones, provides advanced catalytic properties [13]. However, the presence of nitrogen in a LOHC-substrate molecule can lead to the leaching of active sites from the surface of the carbon support as a result of complexation of the Pd:N-heterocycle. Thus, to create catalysts for the dehydrogenation of N-heterocycles with a high stability, it is promising to use g-C_3N_4 as supports that has the content of surface nitrogen reaching 50 at.%. It should be noted that one of the main problems, currently being solved, solved in applications using carbon nitride is the development of techniques for the synthesis of g-C_3N_4 with a high specific surface area. This is due to the fact that ordinary carbon nitride synthesized through melamine pyrolysis is characterized by a low specific surface area (3–5 m^2/g), and to solve a wide range of problems with its use, it is necessary to achieve enhanced textural characteristics of the material. This process is realized during the exfoliation when the layers of graphite-like carbon nitride are separated. In this direction, at the moment, a significant amount of research has been carried out [14] and the obtained exfoliated g-C_3N_4 materials have been tested in detail in a number of photocatalytic processes [9]. The use of exfoliated-g-C_3N_4 materials as carriers for various supported catalysts has been less explored. Nevertheless, there are examples of transesterification [15,16], hydrogenation [17–19] etc. The process of dehydrogenation of H_2-rich N-heterocycles using $Metal^0$/exfoliated-g-C_3N_4 catalysts has not been previously studied. Thus, the purpose of this work was to study the properties of palladium catalysts supported by mesoporous carbon nitride in the dehydrogenation of a promising N-heterocyclic LOHC substrate.

2. Results and Discussion

2.1. Synthesis of Graphite-like Carbon Nitride with a High Specific Surface

Along with photocatalytic applications, carbon nitride has attracted significant attention as a promising carbon support with a high content of surface nitrogen. The conventional synthesis of carbon nitride by melamine carbonization makes it possible to obtain a carbon nanomaterial with a deliberately functionalized surface, which provides many advantages compared to nitrogen free analogs. However, the low specific surface area of g-C_3N_4 has long been a significant limitation both for the development of photocatalytic applications and for the use of g-C_3N_4 as a support for supported catalysts. The first implemented method for improving texture characteristics was the sulfuric acid treatment of g-C_3N_4 [20] by analogy with the Hummers' method for graphite [21]. However, the low manufacturability of this method initiated further research. Methodologies for hard template synthesis during melamine carbonization in the presence of SiO_2, MgO, and melting salts (NaCl-KCl) followed by washing out of the template [22–24] were successively studied. Nevertheless, soft-template methodologies attracted the most attention. Among them, carbonization of the melamine:cyanuric acid adduct [25–27] is considered as the most technologically advanced and scalable in the future [14].

Melamine cyanurate is a adduct compound having the composition $(M_x{:}CA_y)_n$ (Figure 1), which is poorly soluble in most solvents. The methodology for its synthesis consists in mixing solutions of commercially available melamine and cyanuric acid. Subsequent carbonization of the material at 400–550 °C temperatures results in the decomposition of oxygen-containing blocks of the MCA adduct with the formation of a material similar in composition and structure to the g-C_3N_4 materials obtained by pyrolysis of melamine and other precursors.

Preprints (www.preprints.org) | NOT PEER-REVIEWED | Posted: 6 July 2023 doi:10.20944/preprints202307.0410.v1

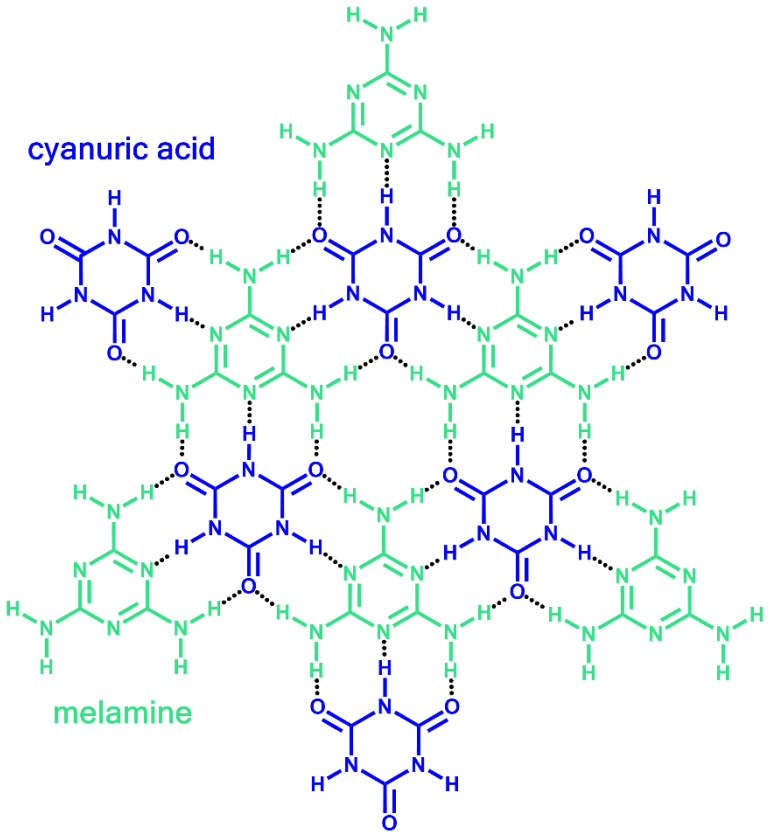

Figure 1. The structure of the melamine:cyanuric acid adduct (melamine cyanurate).

However, the solubility of melamine and cyanuric in water, DMSO or other organic solvents is rather low. Specific surface area of the target carbon nitride significantly depends on the morphology of the starting $(M:CA)_n$, and the smaller crystallite size (<D>) of the adduct provides more developed textural characteristics [27]. This parameter, in turn, depends on the synthesis methodology. In a series of experiments, the influence of a solvent type and the deposition temperature on the characteristics of the resulting nanosols and the specific surface area of the final carbonized MCA was studied (Table 1). Herewith, the single-point BET method was used for the screening study of specific surface area of the synthesized samples of carbonized MCA adducts. Nanosols obtained from low concentration solutions of M and CA in water and DMSO were studied using the dynamic light scattering (DLS) method, in which the hydrodynamic particle diameter was determined. As can be seen from the obtained data (Table 1), there is a certain correlation between the particle size in solution and the specific surface area of the obtained carbon nitride. On Figure 2 as an example, typical particle size distributions for different solutions are given. In the case of a good sample, a small particle size and a minimum content of large aggregates in solution are observed. With an increase in the particle size and/or an increase in the fraction of large aggregates, the values of the obtained specific surface area of the samples during the synthesis decrease.

Table 1. An effect of cyanurate-melamine synthesis methodology on a particle size of MCA and the specific surface area of MCA-derived carbon nitride.

Method	Solutions Used for Precipitation (Solvent, Concentration, Temperature)		<D> in MCA-Solvent Suspension*, nm	SSA** of Calcined (450 °C) Sample, m^2/g
	Melamine (M)	Cyanuric Acid (CA)		
m1	H_2O,	H_2O,	194	61

Preprints (www.preprints.org) | NOT PEER-REVIEWED | Posted: 6 July 2023 doi:10.20944/preprints202307.0410.v1

	~0.2% 25 °C	~0.2% 25 °C		
m2	H_2O, ~2.5%, 90 °C	H_2O, ~2.5%, 90 °C	366	24
m3	DMSO, ~2.5%, 25 °C	DMSO, ~2.5%, 25 °C	130	72
m4	DMSO, ~7.5%, 25 °C	DMSO, ~7.5%, 25 °C	288	34
m5	HCl-H_2O (1M), ~2%, 25 °C	NH_4OH-H_2O (1M), ~2%, 25 °C	201	59

* Particles diameter according to DLS method ** by single-point N_2 adsorption.

An elevated precipitation temperature makes it possible to obtain large amounts of $(M:CA)_n$, which, taking into account the low solubility of the initial reagents, is important for the development of a technological synthesis method. However, it has been shown that an increased precipitation temperature leads to an increase in the MCA average crystallite size and, consequently, to a decrease in the specific surface area of the carbonized product.

The use of dimethyl sulfoxide instead, supposedly provides better solubility, which favorably affects SSA. However, increasing the concentration of melamine and cyanuric acid in DMSO up to the solubility limits also led to the SSA decrease. Also, it was shown that the use of ionic solutions of melamine and cyanuric acid containing, respectively, hydrochloric acid and ammonium hydrate, makes it possible to increase the solubility of the starting compounds. When MCA was precipitated from this solution, <D> values comparable to those of m3 method (Table 1) were achieved. The subsequent separation of the resulting adduct by centrifugation allows for obtaining a carbonized product with an SSA of 59 m^2/g (carbonization temperature 450°C).

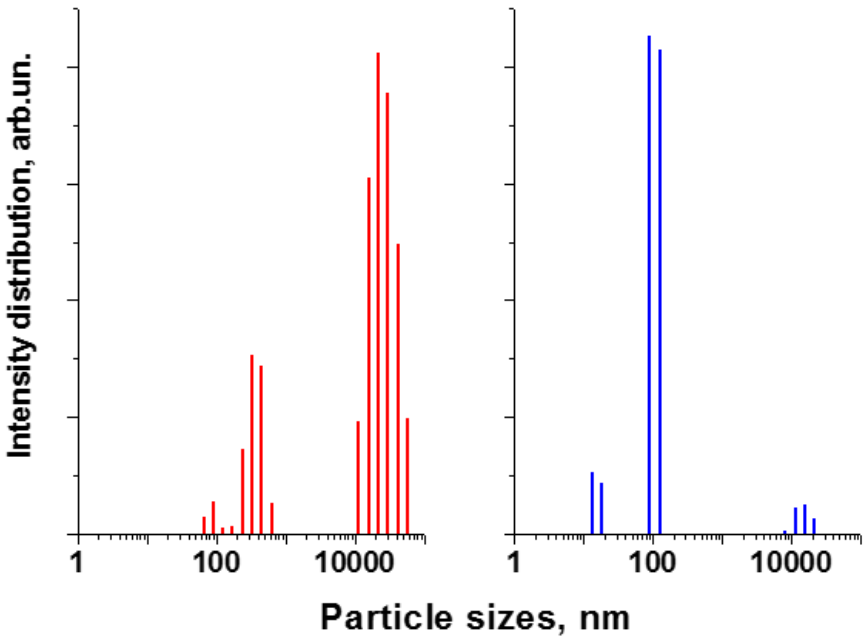

Figure 2. Intensity distribution for the suspensions prepared by m2 (red line) and m3 (blue line) methods.

Preprints (www.preprints.org) | NOT PEER-REVIEWED | Posted: 6 July 2023 doi:10.20944/preprints202307.0410.v1

At the next stage of research, using the method developed for m5, the influence of the carbonization temperature (Table 2, Figure 3) and M:CA ratio (Table 1) on the textural characteristics and the yield of the carbonization product was studied. As a result of the investigation, it was shown that despite a significant increase in the specific surface area at an elevated carbonization temperature, there is a significant decrease in the product yield. In this case, a darkening of the carbonized sample from light to dark gray was noted, which is presumably associated with carburization.

Table 2. Effect of carbonization temperature on the support yield and the BET specific surface area (SSA) of carbon nitride prepared by m5 method.

Carbonization Temperature, °C	Yield of Carbonization Product, %	BET SSA*, m^2/g
300	78	4
400	47	3
450	35	59
500	21	71
550	11	121

* by single-point N_2 adsorption.

According to the SEM data (Figure 3), an increase in carbonization temperature leads to a significant change in the surface morphology of the MCA. In this case, according to EDX data, oxygen-containing fragments are predominantly decomposed with the formation of a material similar in composition to the carbonization product of pure melamine.

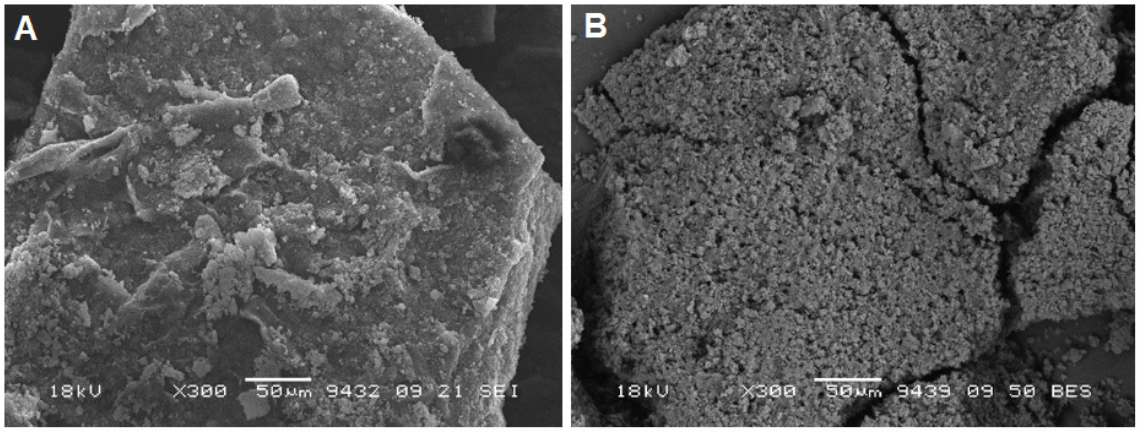

Figure 3. SEM images of samples carbonized at 400 °C (a) and 550 °C (b) demonstrating the effect on the resulting material morphology.

It was shown (Table 3) that a gradual decrease in the content of cyanuric acid leads to an increase in the yield of the carbonization product up to the values typical for the pyrolysis of pure melamine [28].

Table 3. Effect of M:CA ratio on the carbon nitride BET SSA and material yield.

M:CA (mol:mol)	Temperature, °C	Yield of Carbonization Product, %	BET SSA*, m^2/g
1:0	550	34	3
0.9:0.1	500	29	12
0.67:0.33	500	24	41
0.5:0.5	500	21	71

Preprints (www.preprints.org) | NOT PEER-REVIEWED | Posted: 6 July 2023 doi:10.20944/preprints202307.0410.v1

0.6:0.4	500	9	65

* by single-point N_2 adsorption.

The nitrogen adsorption-desorption isotherms on the samples with M:CA ratio of 1:0 and 0.5:0.5 are given in Figure 4. One can see that the isotherms are very similar between each other except the fact that the adsorption on the sample with M:CA=0.5:0.5 becomes several times higher than that of the sample with M:CA=1:0. The both isotherms are of type II with hysteresis H3 according to the classification by IUPAC [29].

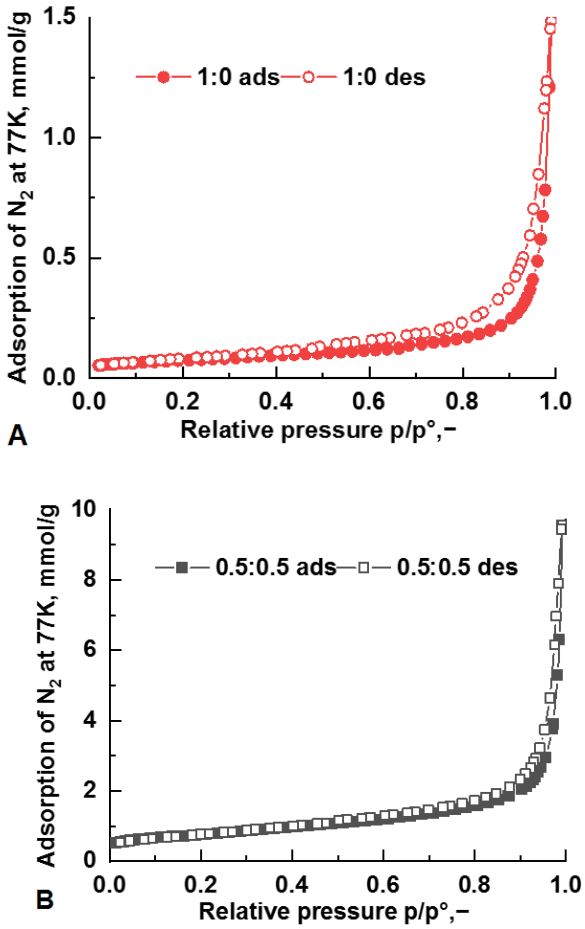

Figure 4. The isotherms of nitrogen adsorption-desorption at 77K on the samples with different content of cyanuric acid (for nomenclature see Table 3) after calcination. A — the sample with M:CA=1:0, B — the sample with M:CA=0.5:0.5.

This type of isotherms is characteristic for macroporous and non-porous samples. Thus, the adding cyanuric acid does not result in the formation of mesopores. The pore size distribution, calculated by using of the BJH method applied to the desorption branch of isotherms, does not show any mesopores as well (Figure 5). The maximum of the differential curve dV/dlogD for the sample M:CA=1:0 is about 50 nm, that for the sample M:CA=0.5:0.5 is ca. 70 nm.

Preprints (www.preprints.org) | NOT PEER-REVIEWED | Posted: 6 July 2023 doi:10.20944/preprints202307.0410.v1

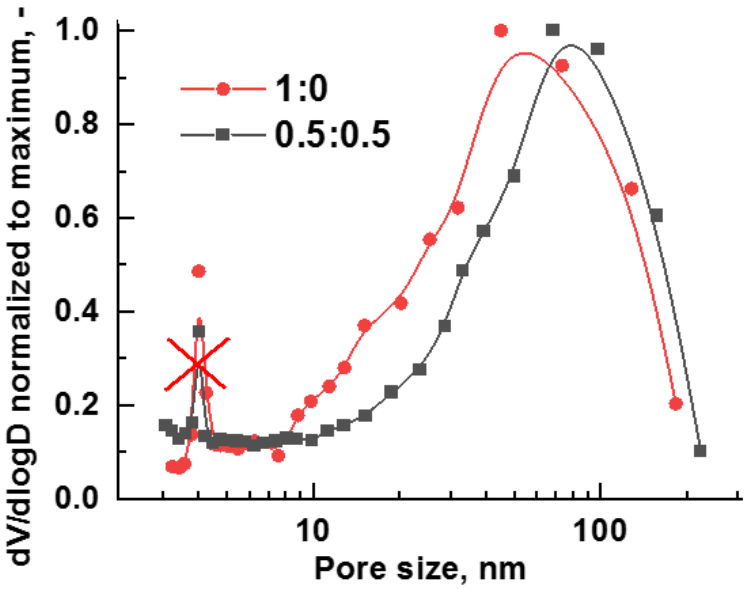

Figure 5. Pore size distribution dV/dlogD normalized to the maximum of this distribution in products of condensation of melamine and cyanuric acid. Calculation by BJH procedure using the desorption branch of isotherms. The peak at 4 nm should be ignored, because it is the widely known artifact of nitrogen adsorption [30].

In contrast to the well-crystallized g-C_3N_4, MCA-550 materials obtained by $(M:CA)_n$ calcination differ significantly in morphology. According to the data of scanning electron microscopy, a greater disorder and a looser structure of the samples are observed upon passing from g-C_3N_4 to MCA-500 (Figure 6).

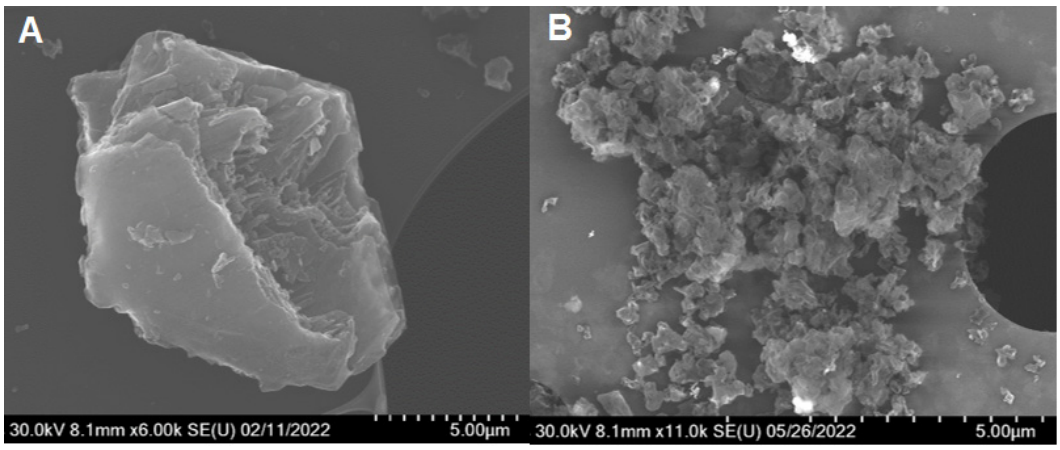

Figure 6. SEM images of g-C_3N_4 and MCA-500 supports.

This conclusion also agrees with the X-ray diffraction data (Figure 7). The diffraction patterns of the g-C_3N_4 and MCA samples show two main reflections at positions 13.2° and 27.3°, which correspond to peaks (100) and (002) in the C_3N_4 structure, respectively. However, the MCA sample is characterized by a more disordered structure, which is explained by larger specific surface area. The most intense reflection (002) refers to the interplanar distances arising from the stacking of graphite-like conjugated triazine aromatic fragments. The determined distance from the magnitude of this reflection is 0.32 nm, which is in good agreement with the data for standard carbon nitride (JCPDS 87–1526). Moreover, wide diffraction peaks for MSA samples in range 22-25° look like diffraction patterns from C_3N_4 nanosheets [31–33]. Probably in the case of MSA sample triazine layers are more disordered compared to usual g-C_3N_4 samples.

Preprints (www.preprints.org) | NOT PEER-REVIEWED | Posted: 6 July 2023 doi:10.20944/preprints202307.0410.v1

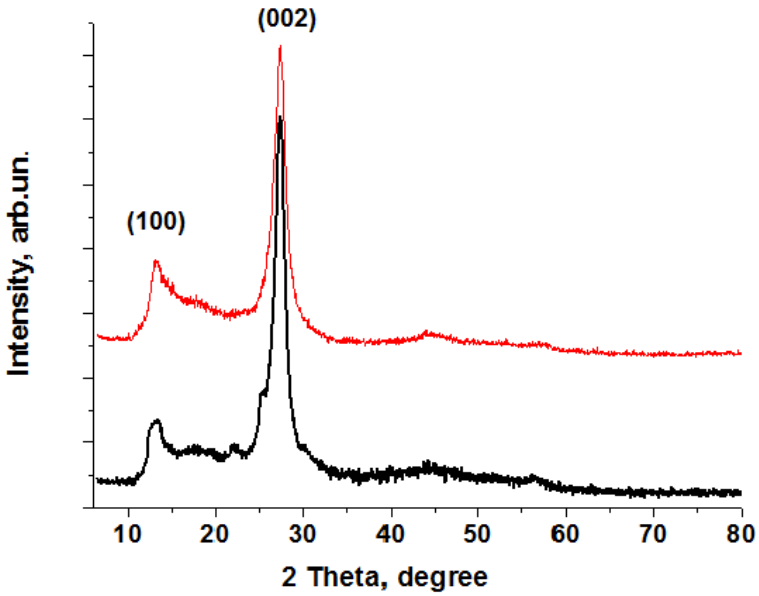

Figure 7. X-ray diffraction patterns of samples (g-C_3N_4 (red line) and MCA (black line)).

According to the SAXS data (Figure 8), all C_3N_4 samples have typical disordering porous structure like usual porous supports without any peculiarities. Furthermore, MCA sample is also characterized by smaller values of structural parameters in comparison with the g-C_3N_4 sample. Thus, for MSA, the value of the correlation length determined from the SAXS data was 38.6 nm, while for the g-C_3N_4 sample, the analogous value was 47.2 nm. The values of specific surface area according to the Porod model were 77 m^2/g for MCA-500 and 29 m^2/g for g-C_3N_4 sample. On the whole, this is in good agreement with the BET data.

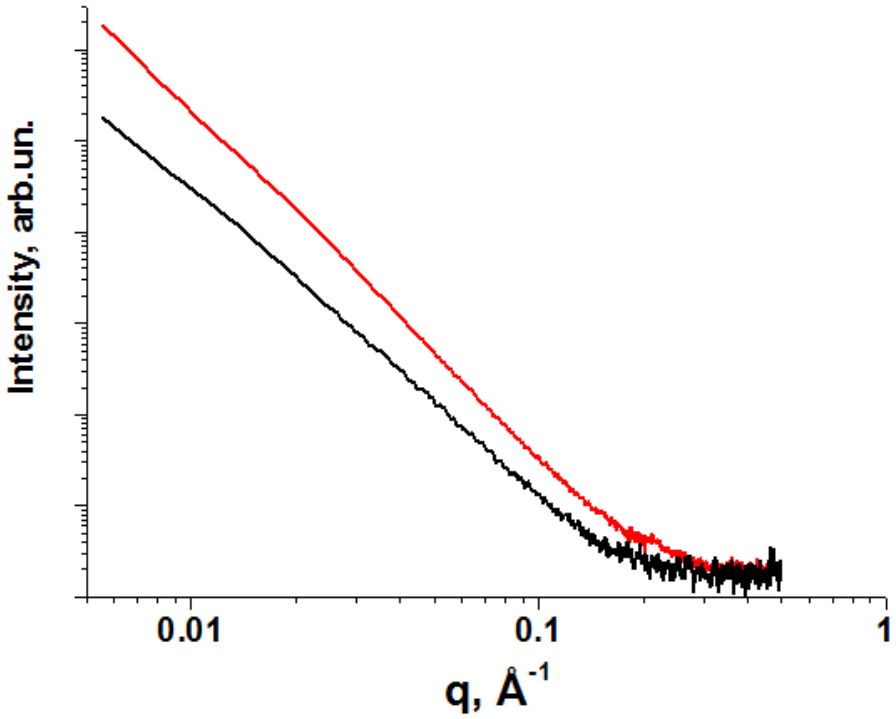

Figure 8. SAXS patterns of samples (g-C_3N_4 (red line) and MCA-500 (black line)).

Preprints (www.preprints.org) | NOT PEER-REVIEWED | Posted: 6 July 2023 doi:10.20944/preprints202307.0410.v1

Using high-resolution transmission electron microscopy, changes in the morphology of particles of the initial $(M:CA)_n$ and graphite-like carbon nitride obtained on its basis were studied. According to the obtained data on micrographs of the original MCA (Figure 9a-9b), elongated particles were found (length - 200-400 nm, thickness - 30-50 nm). After heat treatment, these particles are destroyed via opening into sheets consisting of several layers of carbon nitride. (Figure 9c-9d). According to EDX analysis of studied samples, quantities of C, N and O were equal 50.6±5.9%, 47.6±5.6 and 1.8±0.4% respectively.

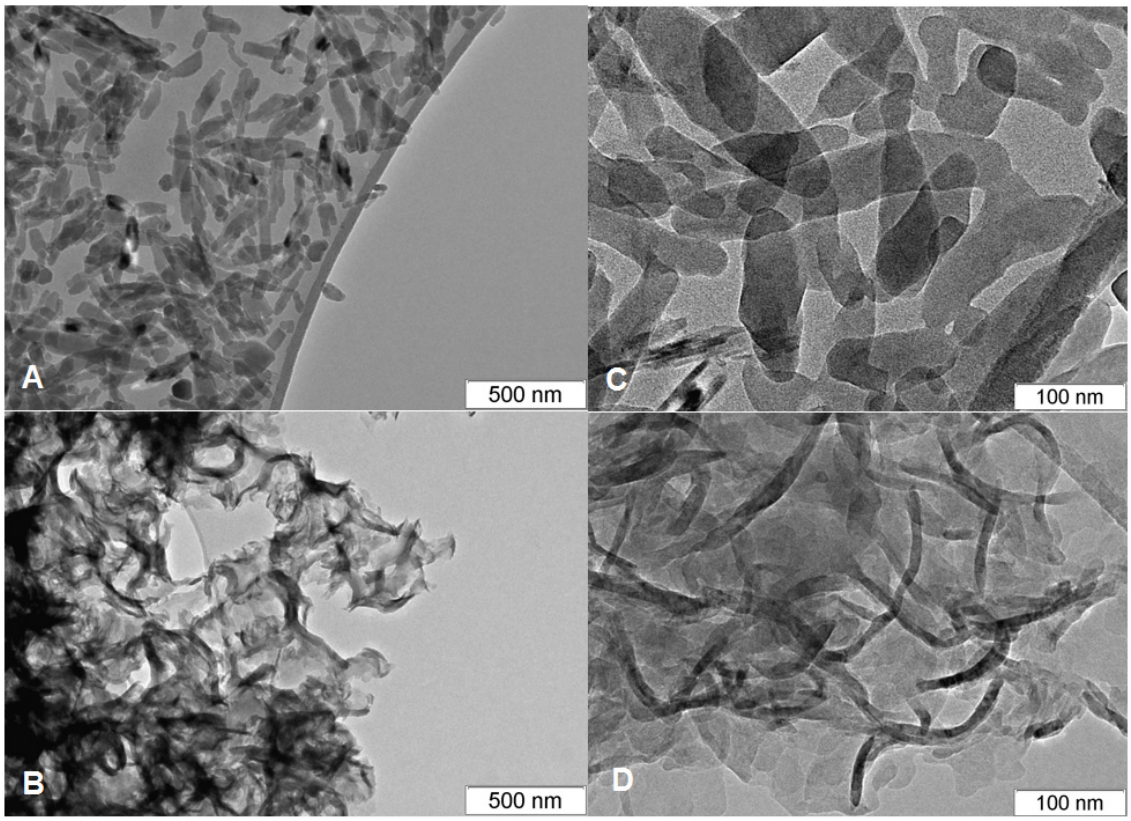

Figure 9. HRTEM images of $(M:CA)_n$ (a-b) and MCA-500 (c-d) samples.

2.2. Investigation of the catalytic activity of Pd/Carbon nitride systems in the decahydroquinoline dehydrogenation

Figure 10 shows the reaction scheme for the stepwise dehydrogenation of decahydroquinoline using synthesized palladium-containing catalysts. The reaction takes place with the formation of intermediates – 1,2,3,4-tetrahydroquinoline (4HQc) and 5,6,7,8-tetrahydroquinoline (4HQn). In this case, according to the GC data of the reaction mixtures, the contribution of the route through 4HQn is not significant that agrees with the previously obtained data for $Pd/\gamma\text{-}Al_2O_3$ catalysts [5]. This is due to the significantly higher dehydrogenation rate of the nitrogen-containing quinoline ring (ΔG_f = 49.6 kJ/mol, according to the calculated data [5]), as compared to the carbon ring (64.5).

Preprints (www.preprints.org) | NOT PEER-REVIEWED | Posted: 6 July 2023 doi:10.20944/preprints202307.0410.v1

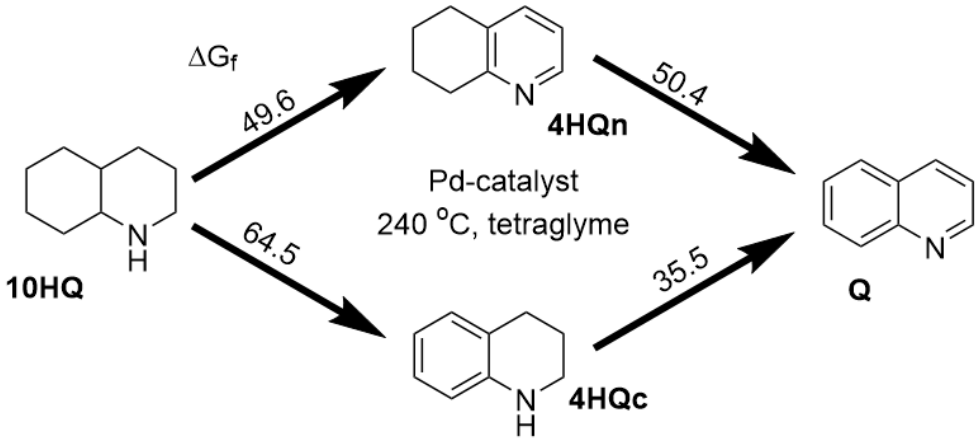

Figure 10. A scheme of decahydroquinoline dehydrogenation.

As the main parameter for evaluating the catalytic activity of the Pd/g-C_3N_4 samples under study and the Pd/C reference catalyst, we used the yield of hydrogen from the theoretically possible value for 1 hour of reaction. The chromatograms of the reaction mixtures showed tetraglyme (solvent), decahydroquinoline (initial substrate) and dehydrogenation products, with insignificant (<1 mol.%) admixture of 1,2,3,4-tetrahydroquinoline. It should be noted that for all catalytic tests using carbon supports (g-C_3N_4, MCA, C), no by-products of decahydroquinoline decomposition, as well as products of substitution of the N-heterocycle by alkyl fragments, were detected on the chromatograms of the reaction mixtures. In turn, when Pd/γ-Al_2O_3 was used, the content of N-methyl- and N-ethyl-1,2,3,4-tetrahydroquinolines was noted in the reaction mixtures (less than 0.5 mol % in total). This is presumably related to the process of alkylation of the N-heterocycle by the decomposition products of the reaction solvent (tetraglyme), which occurs on the alumina acid sites.

It has been shown that the use of wet impregnation technique (wi, Table 4) generally results in less efficient catalysts for 10HQ dehydrogenation. Although the catalysts comparable in activity (ai-1%Pd/g-C_3N_4 ~ wi-1%Pd/g-C_3N_4) were obtained using standard low-surface g-C_3N_4, the ai-1%Pd/MCA-500 catalyst is significantly superior in activity wi-1%Pd/ISA-500. Presumably, in the case of the exfoliated support g-C_3N_4, wet impregnation does not allow one to obtain catalysts with a high dispersion of the supported metal. The hydrogen yield when using ai-1%Pd/MCA-500 (M:CA=1) significantly exceeds the similar parameter for 1%Pd/MCA-500 samples with a large M:CA ratio, which is, probably, due to the lower disorder of the exfoliated layers of carbon nitride.

According to high-resolution electron microscopy data, the ai-1%Pd/MCA-500 catalyst contains Pd nanoparticles with sizes from 0.5 to 4 nm. The presence of single palladium atoms fixed on the surface can also be seen in the TEM images. In this case, individual palladium atoms were not used in the construction of the particle size histogram due to the low contrast. The average particle size of palladium was 1.6±0.6 nm. It is interesting to note that, according to the data of CO chemisorption, the dispersity of Pd supported on carbon nitride does not exceed 30% (Table 4). Such dispersion in terms of CO chemisorption should correspond to much larger metal particles with sizes of ≈4 nm [34]. At the same time, it was shown in that CO is not effective adsorbed onto very small clusters and individual palladium atoms, which leads to an underestimation of the dispersion of supported palladium according to CO chemisorption data [35]. Therefore such discrepancy between different methods is only confirm formation of extra small Pd nanoparticles, clusters and single atoms on carbon nitride support.

Preprints (www.preprints.org) | NOT PEER-REVIEWED | Posted: 6 July 2023 doi:10.20944/preprints202307.0410.v1

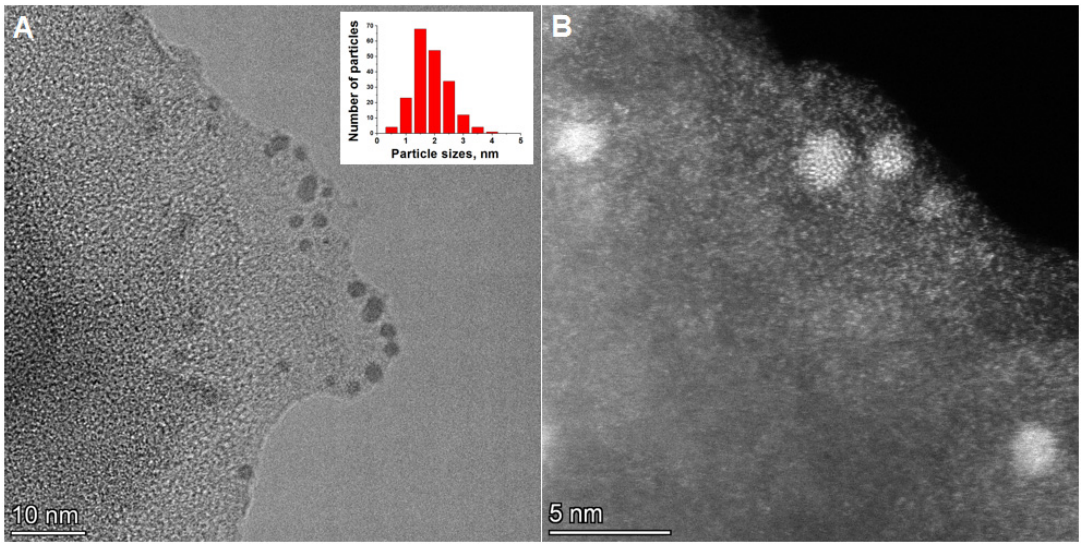

Figure 11. HRTEM images of 1%Pd/MCA-500.

Table 4. Catalytic activity of Pd-containing catalysts in dehydrogenation of decahydroquinoline.

Catalyst	Impregnation Method	M:CA Ratio (mol:mol)	D_{CO}, %	Y_{H2}, %
g-C_3N_4 or MCA -550	-	-	-	0
1%Pd/g-C_3N_4	wi	1:0	17	45
1%Pd/g-C_3N_4	ai	1:0	18	43
1%Pd/MCA -500	wi	(1:1)	20	58
1%Pd/MCA -500	ai	(1:1)	30	94
1%Pd/ MCA -400	ai	(1:1)	-**	12
1%PdMCA -500	ai	(0.67:0.33)	22	71
1%Pd/MCA -500	ai	(0.9:0.1)	20	50
1%Pd/C	-*	-	41	78

*commercial catalyst **not measured.

3. Materials and Methods

3.1. Synthesis of the g-C_3N_4 and MCA-T Supports

The reagents melamine and cyanuric acid (all Alfa Aesar, >99.9%), hydrochloric acid, aqueous ammonia (all Reakhim, 38 and 25 %, respectively) were used as received.

For the synthesis of standard graphite-like nitride (g-C_3N_4), melamine was calcined in a closed alumina crucible at a temperature of 550 °C (4 h) followed by the cooling of the sample for 1 h in an inert atmosphere. The synthesis of graphite-like carbon nitride with improved textural characteristics (MCA-T samples) from MCA adducts was carried out similarly. For the carbonization, the adducts obtained by mixing solutions of melamine and cyanuric acid with vigorous stirring were used. The adducts with various M:CA ratios and precipitated from various solvents were used, the carbonization temperatures were also varied (T = 400 – 600 °C). The yield of the carbonization product was estimated as the percentage of the obtained solid product to the total mass of the initial adduct.

3.2. Synthesis of Pd-Containing Catalytic Systems

For the synthesis of 1 wt% Pd/g-C_3N_4 or 1 wt% Pd/MCA-T catalysts, the wet impregnation and adsorption precipitation techniques were applied using $H_2[PdCl_4]$ as the active component precursor. In the case of wet impregnation, the calculated volume of a solution of palladium salt with a concentration required for the preparation of 1 wt.% of the catalyst was used. Next, the sample was

 doi:10.20944/preprints202307.0410.v1

dried at 100 °C (2 h) and reduced using 1 M solution of sodium borohydride (Fluka). The resulting catalyst was washed with distilled water on a filter and dried at 100°C (2 h).

Using adsorption precipitation technique, 1 g of the support was dispersed in 20 ml of an EDTA water solution (56 mg) using a magnetic stirrer (600 rpm). Then, 1M aqueous solution of $H_2[PdCl_4]$ of the required concentration was added dropwise and stirred for six hours (600 rpm). After that, 5 ml of a 1M sodium borohydride solution was added dropwise to the suspension, which further was stirred for 2 hours, filtered and dried at a temperature of 100 °C (2 hours).

In addition an 1 wt.% Pd/C catalyst sample was used as a prototype one, that was synthesized according to the technique developed at Boreskov Institute of Catalysis [36–38].

3.3. Characterization Techniques

3.3.1. Dynamic Light Scattering (DLS)

Dynamic light scattering experiments were carried out using Photocor equipment (Photocor Instruments, Inc., Moscow, Russia) with a digital correlator (288 channels). The measurements were performed at a scattering angle of 90° and temperature of 24°C. Wavelength of the light source was equal to 638 nm. The processing of the DLS raw data were performed using the DynaLS software [39]. For calculation of particle sizes, standard values of viscosity and refractive index H_2O and DMSO were used. To calculate the z-averaged hydrodynamic diameter, we used the Stokes–Einstein formula for spherical particles [40].

3.3.2. Electron Microscopy (SEM and TEM)

SEM measurements were performed using Hitachi Regulus SU8230 (Japan) electron microscope with electron beam energy of 30 keV in Secondary Electrons (SE) detection and Dark Field Scanning Transmission Electron Microscope (DF-STEM) modes.

The dispersion of metal particles and the microstructure of the catalysts were studied by transmission electron microscopy. The images were acquired with a JEM-2010 (JEOL Ltd., Tokyo, Japan) operating at an accelerating voltage of 200 kV and a resolution of 0.14 nm.

3.3.3. Adsorption Measurements (CO Chemisorption and BET)

The CO chemisorption was measured in a pulsed mode using a Chemosorb analyzer (MBE, Novosibirsk, Russia) equipped with a thermal conductivity detector. The catalyst (50 mg) was loaded into a U-shaped quartz reactor and treated with an H_2 flow (100 ml/min) at 20 and 100 °C with a heating rate of 10 °C/min. The reactor was kept at the final temperature for 20 min, then purged with argon and cooled to room temperature. After cooling, CO pulses (0.1 cm^3) were injected into the reactor until the sample was saturated, and the amount of chemisorbed CO was estimated.

Single-point BET measurements of surface area were performed by dynamic adsorption of nitrogen at 77K. The adsorption in BET range was made by means of dynamic adsorption analyzer Sorbtometr (Katakon LLC, Novosibirsk, Russia). Prior to the measurements, all samples were degassed in helium flow at 150 °C for 2 h.

Porous structure was studied by nitrogen adsorption-desorption at 77 K. The isotherms were measured by means of an automatic adsorption analyzer Autosorb-6B (Quantachrome Instruments, Boynton Beach, FL, USA). Before the measurements, all samples were degassed in vacuum less than 1 Pa at 150 °C for 16 h.

3.3.4. X-ray Diffraction (XRD)

Powder XRD measurements were carried out using a ARL X'TRA diffractometer (Thermo Electron Corporation, Switzerland), equipped with the vertical theta-theta geometry (Bragg–Brentano), CuKα radiation (λ=0.15418 nm) and a Peltier cooled Si(Li) solid state detector. A 2θ range from 10° to 80° was scanned with a step of 0.05° and counting time of 5 s.

Preprints (www.preprints.org) | NOT PEER-REVIEWED | Posted: 6 July 2023 doi:10.20944/preprints202307.0410.v1

3.3.5. Small Angle X-ray Scattering (SAXS)

S3 MICRO (HECUS) small angle diffractometer (Cu Kα, 50W) with a point collimation of primary beam was used for measuring scattering patterns of all samples. The scattering vector magnitude $q = 4\pi*\sin(\theta)/\lambda$ (where 2θ is the scattering angle, and λ = 1.541 E is the radiation wavelength) was used as the scattering coordinate. The scattering intensity was measured in the range of the scattering vector magnitudes $0.01 < q < 0.60$ E^{-1}. The data processing of the scattering curves was performed using the ATSAS software [41]. Structural invariants such as correlation length and Porod specific surface have been calculated by using special formulas [42].

3.3.6. Elemental Analysis

The Pd concentration in the fresh and exhaust catalysts was determined using an ARL Advant'X 2247 X-ray fluorescence spectrometer (Thermo Fisher Scientific Inc.)

3.4. Catalytic Activity Tests

The catalytic activity of the synthesized Pd-containing catalysts, as well as the prototypical 1% Pd/C catalysts, was studied in the decahydroquinoline dehydrogenation reaction. Decahydroquinoline was preliminarily synthesized from a commercially available quinoline (Sigma Aldrich, St. Louis, MO, USA) according to the earlier described method [5]. 1H-NMR and GC-MS methods confirmed the purity of the obtained N-heterocyclic substrate (more than 99.7%). To study decahydroquinoline dehydrogenation, a reaction setup similar to those described earlier [5] was used.

The study of catalytic activity was carried out similarly to our previous reports [5, 43]. In a standard test of the catalytic activity, the catalyst (50 mg) and a suspension of 1 mmol decahydroquinoline in tetraglyme (3 ml) (Acros Organics, Geel, Belgium) were loaded into the reactor. The system was purged with argon (20 mL/min, 5 min, room temperature) the reactor was sealed, and connected to the system for measuring the volume of released hydrogen. Next, the reaction mixture was heated to 240 °C with stirring (500 rpm) for 15 min (0–900 s) and the dehydrogenation reaction was carried out for 45 min (900–3600 s) before the reactor was removed from the heating zone. Then, the selected aliquot of the reaction mixture was separated from the catalyst particles by centrifugation and analyzed by the GC method. The GC analysis was performed using an Agilent-7890A gas chromatograph (Santa Clara, CA, USA) equipped with a ZB-5HT column.

The hydrogen yield characterizing the depth of dehydrogenation was calculated as follows:

$$Y_{H2} = Y_Q + 0.6\cdot(Y_{4HQc} + Y_{4HQn}), \% \quad (1)$$

where Y_Q Y_{4HQc} and Y_{4HQn} are the molar fractions of the product (Y_Q) and intermediates (Y_{4HQc} and Y_{4HQn}) obtained by gas chromatography.

4. Conclusions

Thus, a series of exfoliated carbon nitrides MCA-T were synthesized from melamine cyanurate with a specific surface area up to 121 m^2/g. Based on the data on the yield of the carbonization product, the optimal support synthesis temperature and the M:CA ratio were selected. The MSA-500 support was used for the synthesis of a palladium-containing catalyst. It has been shown that the use of the adsorption precipitation technique allows for obtaining 1 wt% Pd/MCA-500 catalysts with an ultrafine distribution of palladium, in which this noble metal is represented by atomic and 1-2 nm Pd particles. The synthesized samples were studied in dehydrogenation of decahydroquinoline and it was shown that the 1 wt% Pd/MCA-500 catalyst is significantly superior in activity (94% hydrogen yield per reaction hour) to the low-surface analog 1 wt% Pd/g-C_3N_4 (45%) and prototype 1 wt% Pd/C (78%) catalysts.

Funding: This research was funded by the Ministry of Science and Higher Education of the Russian Federa-tion within the governmental order for Boreskov Institute of Catalysis (project AAAA-A21-121011390007-7 and AAAA-A21-121011390053-4).

Acknowledgments : The authors are grateful to Ms. Daria A. Ovchinnikova, Mr. Maxim G. Dubina and Ms. Viktoriya S. Patrusheva (all from Novosibirsk State Technical University) for assisting in the synthetic procedures; Mrs. Aleksandra N. Serkova from Boreskov Institute of Catalysis for SEM studies; Dr. Evgeniy Yu. Gerasimov from Boreskov Institute of Catalysis for TEM studies; Dr. Sergey E. Malykhin and Prof. Aleksandr M. Volodin from Boreskov Institute of Catalysis for the fruitful discussion.

Conflicts of Interest: The authors declare no conflict of interest.

References

1. Makaryan, I.A.; Sedov, I. V.; Maksimov, A.L. Hydrogen Storage Using Liquid Organic Carriers. *Russ. J. Appl. Chem.* **2020**, *93*, 1815–1830, doi:10.1134/S1070427220120034.
2. Alekseeva (Bykova), M. V.; Gulyaeva, Y.K.; Bulavchenko, O.A.; Saraev, A.A.; Kremneva, A.M.; Stepanenko, S.A.; Koskin, A.P.; Kaichev, V. V.; Yakovlev, V.A. Promoting Effect of Zn in High-Loading Zn/Ni-SiO_2 Catalysts for Selective Hydrogen Evolution from Methylcyclohexane. *Dalt. Trans.* **2022**, *51*, 6068–6085, doi:10.1039/d2dt00332e.
3. Safronov, S.P.; Vostrikov, S. V.; Samarov, A.A.; Wasserscheid, P.; Müller, K.; Verevkin, S.P. Comprehensive Thermodynamic Study of Substituted Indoles/Perhydro Indoles as Potential Liquid Organic Hydrogen Carrier System. *Fuel* **2023**, *331*, 125764, doi:10.1016/j.fuel.2022.125764.
4. Vostrikov, S. V.; Konnova, M.E.; Turovtzev, V. V.; Müller, K.; Verevkin, S.P. Thermodynamics of Hydrogen Storage: Equilibrium Study of the LOHC System Indole/Octahydroindole. *Fuel* **2023**, *335*, 127025, doi:10.1016/j.fuel.2022.127025.
5. Stepanenko, S.A.; Shivtsov, D.M.; Koskin, A.P.; Koskin, I.P.; Kukushkin, R.G.; Yeletsky, P.M.; Yakovlev, V.A. N-Heterocyclic Molecules as Potential Liquid Organic Hydrogen Carriers: Reaction Routes and Dehydrogenation Efficacy. *Catalysts* **2022**, *12*, doi:10.3390/catal12101260.
6. Verevkin, S.P.; Safronov, S.P.; Samarov, A.A.; Vostrikov, S. V. Hydrogen Storage: Thermodynamic Analysis of Alkylquinolines and Alkylpyridines as Potential Liquid Organic Hydrogen Carriers (LOHC). *Appl. Sci.* **2021**, *11*, doi:10.3390/app112411758.
7. Gupta, A.; Likozar, B.; Jana, R.; Chanu, W.C.; Singh, M.K. A Review of Hydrogen Production Processes by Photocatalytic Water Splitting – From Atomistic Catalysis Design to Optimal Reactor Engineering. *Int. J. Hydrogen Energy* **2022**, *47*, 33282–33307, doi:10.1016/j.ijhydene.2022.07.210.
8. Zheng, D.; Xue, Y.; Wang, J.; Varbanov, P.S.; Klemeš, J.J.; Yin, C. Nanocatalysts in Photocatalytic Water Splitting for Green Hydrogen Generation: Challenges and Opportunities. *J. Clean. Prod.* **2023**, *414*, doi:10.1016/j.jclepro.2023.137700.
9. Ye, S.; Wang, R.; Wu, M.Z.; Yuan, Y.P. A Review on g-C_3N_4 for Photocatalytic Water Splitting and CO_2 Reduction. *Appl. Surf. Sci.* **2015**, *358*, 15–27, doi:10.1016/j.apsusc.2015.08.173.
10. Murugan Arunachalapandi; Selvaraj Mohana Roopan Environment Friendly g-C_3N_4-Based Catalysts and Their Recent Strategy in Organic Transformations. *High Energy Chem.* **2022**, *56*, 73–90, doi:10.1134/S0018143922020102.
11. Li, X.H.; Wang, X.; Antonietti, M. Mesoporous g-C_3N_4 Nanorods as Multifunctional Supports of Ultrafine Metal Nanoparticles: Hydrogen Generation from Water and Reduction of Nitrophenol with Tandem Catalysis in One Step. *Chem. Sci.* **2012**, *3*, 2170–2174, doi:10.1039/c2sc20289a.
12. Chen, H.; Shuang, H.; Lin, W.; Li, X.; Zhang, Z.; Li, J.; Fu, J. Tuning Interfacial Electronic Properties of Palladium Oxide on Vacancy-Abundant Carbon Nitride for Low-Temperature Dehydrogenation. *ACS Catal.* **2021**, *11*, 6193–6199, doi:10.1021/acscatal.1c00712.
13. Suominen, M.; Kallio, T. What We Currently Know about Carbon-Supported Metal and Metal Oxide Nanomaterials in Electrochemical CO_2 Reduction. *ChemElectroChem* **2021**, *8*, 2397–2406, doi:10.1002/celc.202100345.
14. Barrio, J.; Shalom, M. Rational Design of Carbon Nitride Materials by Supramolecular Preorganization of Monomers. *ChemCatChem* **2018**, *10*, 5573–5586, doi:10.1002/cctc.201801410.
15. Xu, J.; Long, K.Z.; Wang, Y.; Xue, B.; Li, Y.X. Fast and Facile Preparation of Metal-Doped g-C_3N_4 Composites for Catalytic Synthesis of Dimethyl Carbonate. *Appl. Catal. A Gen.* **2015**, *496*, 1–8, doi:10.1016/j.apcata.2015.02.025.
16. Xu, J.; Chen, Y.; Ma, D.; Shang, J.K.; Li, Y.X. Simple Preparation of MgO/g-C_3N_4 Catalyst and Its Application for Catalytic Synthesis of Dimethyl Carbonate via Transesterification. *Catal. Commun.* **2017**, *95*, 72–76, doi:10.1016/j.catcom.2017.03.009.
17. Zhang, L.; Zhang, L.; Cheng, S.; Zhou, X.; Shang, N.; Gao, S.; Wang, C. Pd Supported on Graphene Modified G-C_3N_4 Hybrid: A Highly Efficient Catalyst for Hydrogenation of Nitroarenes. *Appl. Organomet. Chem.* **2020**, *34*, 1–9, doi:10.1002/aoc.5684.

18. Payra, S.; Banerjee, S. Highly Efficient and Chemoselective Reduction of Nitroarenes Using Hybrid Ni@g-C_3N_4 as Reusable Catalyst. *ChemistrySelect* **2019**, *4*, 9556–9561, doi:10.1002/slct.201902854.
19. Li, J.; Zahid, M.; Sun, W.; Tian, X.; Zhu, Y. Synthesis of Pt Supported on Mesoporous g-C_3N_4 Modified by Ammonium Chloride and Its Efficiently Selective Hydrogenation of Furfural to Furfuryl Alcohol. *Appl. Surf. Sci.* **2020**, *528*, 146983, doi:10.1016/j.apsusc.2020.146983.
20. Kang, H.J.; Lee, T.G.; Bari, G.A.K.M.R.; Seo, H.W.; Park, J.W.; Hwang, H.J.; An, B.H.; Suzuki, N.; Fujishima, A.; Kim, J.H.; et al. Sulfuric Acid Treated g-CN as a Precursor to Generate High-Efficient g-CN for Hydrogen Evolution from Water under Visible Light Irradiation. *Catalysts* **2021**, *11*, 1–13, doi:10.3390/catal11010037.
21. Feng, J.; Chen, T.; Liu, S.; Zhou, Q.; Ren, Y.; Lv, Y.; Fan, Z. Improvement of G-C3N4 Photocatalytic Properties Using the Hummers Method. *J. Colloid Interface Sci.* **2016**, *479*, 1–6, doi:10.1016/j.jcis.2016.06.040.
22. Jiang, T.; Han, H.; Dong, M.; Zhao, Q. In Situ Construction of Porous g-C_3N_4 Isotype Heterojunction/BiOBr Nanosheets Ternary Composite Catalyst for Highly Efficient Visible-Light Photocatalytic Activity. *ChemistrySelect* **2021**, *6*, 6212–6222, doi:10.1002/slct.202101095.
23. Cheng, M.; Lv, P.; Zhang, X.; Xiong, R.; Guo, Z.; Wang, Z.; Zhou, Z.; Zhang, M. A New Active Species of Pd-Nx Synthesized by Hard-Template Method for Efficiently Catalytic Hydrogenation of Nitroarenes. *J. Catal.* **2021**, *399*, 182–191, doi:10.1016/j.jcat.2021.05.016.
24. Dong, J.; Zhang, Y.; Hussain, M.I.; Zhou, W.; Chen, Y.; Wang, L.N. g-C_3N_4: Properties, Pore Modifications, and Photocatalytic Applications. *Nanomaterials* **2022**, *12*, 1–35, doi:10.3390/nano12010121.
25. Jun, Y.S.; Lee, E.Z.; Wang, X.; Hong, W.H.; Stucky, G.D.; Thomas, A. From Melamine-Cyanuric Acid Supramolecular Aggregates to Carbon Nitride Hollow Spheres. *Adv. Funct. Mater.* **2013**, *23*, 3661–3667, doi:10.1002/adfm.201203732.
26. Dante, R.C.; Martín-Ramos, P.; Correa-Guimaraes, A.; Martín-Gil, J. Synthesis of Graphitic Carbon Nitride by Reaction of Melamine and Uric Acid. *Mater. Chem. Phys.* **2011**, *130*, 1094–1102, doi:10.1016/j.matchemphys.2011.08.041.
27. Zhou, C.; Shi, R.; Shang, L.; Wu, L.-Z.; Tung, C.-H.; Zhang, T. Template-Free Large-Scale Synthesis of g-C_3N_4 Microtubes for Enhanced Visible Light-Driven Photocatalytic H2 Production. *Nano Res.* **2018**, *11*, 3462–3468, doi:10.1007/s12274-018-2003-2.
28. Wang, X.; Han, D.; Ding, Y.; Liu, J.; Cai, H.; Jia, L.; Cheng, X.; Wang, J.; Fan, X. A Low-Cost and High-Yield Approach for Preparing g-C_3N_4 with a Large Specific Surface Area and Enhanced Photocatalytic Activity by Using Formaldehyde-Treated Melamine. *J. Alloys Compd.* **2020**, *845*, 156293, doi:10.1016/j.jallcom.2020.156293.
29. Thommes, M.; Kaneko, K.; Neimark, A. V.; Olivier, J.P.; Rodriguez-Reinoso, F.; Rouquerol, J.; Sing, K.S.W. Physisorption of Gases, with Special Reference to the Evaluation of Surface Area and Pore Size Distribution (IUPAC Technical Report). *Pure Appl. Chem.* **2015**, *87*, 1051–1069, doi:10.1515/pac-2014-1117.
30. Gregg, S. J.; Sing, K. S. W. *Adsorption, Surface Area, & Porosity, Second Edition*, 2nd ed.; Academic Press: London, 1982.
31. Rashidizadeh, A.; Ghafuri, H.; Esmaili Zand, H.R.; Goodarzi, N. Graphitic Carbon Nitride Nanosheets Covalently Functionalized with Biocompatible Vitamin B1: Synthesis, Characterization, and Its Superior Performance for Synthesis of Quinoxalines. *ACS Omega* **2019**, *4*, 12544–12554, doi:10.1021/acsomega.9b01635.
32. Liu, S.; Guo, Z.; Zeng, X.; Meng, X.; Sun, H.; Wan, Y.; Zuo, G. Self Assembly and Controlled Drug Release of a Nano-Laminated Graphite Carbon Nitride/Methotrexate Complex. *J. Mater. Sci. Mater. Med.* **2018**, *29*, 1–6, doi:10.1007/s10856-018-6128-3.
33. Dante, R.C.; Martín-Ramos, P.; Sánchez-Arévalo, F.M.; Huerta, L.; Bizarro, M.; Navas-Gracia, L.M.; Martín-Gil, J. Synthesis of Crumpled Nanosheets of Polymeric Carbon Nitride from Melamine Cyanurate. *J. Solid State Chem.* **2013**, *201*, 153–163, doi:10.1016/j.jssc.2013.02.016.
34. Bergeret, G.; Gallezot, P. Pore Size Distribution and Porosity of Solid Materials by Mercury Porosimetry and Gas Adsorption-Part 2: Analysis of Macropores by Mercury Porosimetry. *96. H. Giesche, Mater. Res. Soc. Symp. Proc* **1991**, *37*, 225.
35. Arrigo, R.; Schuster, M.E.; Xie, Z.; Yi, Y.; Wowsnick, G.; Sun, L.L.; Hermann, K.E.; Friedrich, M.; Kast, P.; Hävecker, M.; et al. Nature of the N-Pd Interaction in Nitrogen-Doped Carbon Nanotube Catalysts. *ACS Catal.* **2015**, *5*, 2740–2753, doi:10.1021/acscatal.5b00094.
36. Simakova, I.; Koskin, A.; Deliy, I.; Simakov, A. Nanoscaled Palladium Catalysts on Activated Carbon Support "Sibunit" for Fine Organic Synthesis. *Complex Mediu. VI Light Complex.* **2005**, *5924*, 592413, doi:10.1117/12.616317.
37. Koskin, A.P.; Simakova, I.L.; Parmon, V.N. Reductive Debenzylation of Hexabenzylhexaazaisowurtzitane — the Key Step of the Synthesis of Polycyclic Nitramine Hexanitrohexaazaisowurtzitane. *Russ. Chem. Bull.* **2007**, *56*, 2370–2375, doi:10.1007/s11172-007-0377-5.

38. Koskin, A.P.; Simakova, I.L.; Parmon, V.N. Study of Palladium Catalyst Deactivation in Synthesis of 4,10-Diformyl-2,6,8,12-Tetraacetyl-2,4,6,8,10,12-Hexaazaisowurtzitane. *React. Kinet. Catal. Lett.* **2007**, *92*, 293–302, doi:10.1007/s11144-007-5203-4.
39. http://www.softscientific.com/science/WhitePapers/dynals1/dynals100.htm.
40. Hassan, P.A.; Rana, S.; Verma, G. Making Sense of Brownian Motion: Colloid Characterization by Dynamic Light Scattering. *Langmuir* **2015**, *31*, 3–12, doi:10.1021/la501789z.
41. Konarev, P. V.; Petoukhov, M. V.; Volkov, V. V.; Svergun, D.I. ATSAS 2.1, a Program Package for Small-Angle Scattering Data Analysis. *J. Appl. Crystallogr.* **2006**, *39*, 277–286, doi:10.1107/S0021889806004699.
42. Feigin, L.A.; Svergun, D.I. *Structure Analysis by Small-Angle X-Ray and Neutron Scattering*; Taylor, G.W., Ed.; Springer US: Boston, MA, 1987; ISBN 978-1-4757-6626-4.
43. Shivtsov, D.M.; Koskin, A.P.; Stepanenko, S.A.; Ilyina, E.V.; Ayupov, A.B.; Bedilo, A.F.; Yakovlev, V.A. Hydrogen Production by N-Heterocycle Dehydrogenation over Pd Supported on Aerogel-Prepared Mg-Al Oxides. *Catalysts* **2023**, *13*, 10.3390/catal13020334.